Irreducible correlation functions of the $\hat{S}$ matrix in the coordinate representation: Application in calculating Lorentzian half-widths and shifts

Q. Ma[a)]
NASA/Goddard Institute for Space Studies and Department of Applied Physics and Applied Mathematics, Columbia University, New York, New York 10025

R. H. Tipping
Department of Physics and Astronomy, University of Alabama, Tuscaloosa, Alabama 35487

C. Boulet
Laboratoire Inter-Universitaire des Systèmes Atmosphériques (LISA), CNRS, Universités Paris 12 et 7, 61 Avenue Général de Gaulle, 94010 Crèteil-Cedex, France; and Laboratoire de Photophysique Moléculaire, Université Paris-Sud, Centre 91405 Orsay Cedex, France

(Received 6 September 2005; accepted 28 October 2005; published online 5 January 2006)

By introducing the coordinate representation, the derivation of the perturbation expansion of the Liouville $\hat{S}$ matrix is formulated in terms of classically behaved autocorrelation functions. Because these functions are characterized by a pair of irreducible tensors, their number is limited to a few. They represent how the overlaps of the potential components change with a time displacement, and under normal conditions, their magnitudes decrease by several orders of magnitude when the displacement reaches several picoseconds. The correlation functions contain all dynamical information of the collision processes necessary in calculating half-widths and shifts and can be easily derived with high accuracy. Their well-behaved profiles, especially the rapid decrease of the magnitude, enables one to transform easily the dynamical information contained in them from the time domain to the frequency domain. More specifically, because these correlation functions are well time limited, their continuous Fourier transforms should be band limited. Then, the latter can be accurately replaced by discrete Fourier transforms and calculated with a standard fast Fourier transform method. Besides, one can easily calculate their Cauchy principal integrations and derive all functions necessary in calculating half-widths and shifts. A great advantage resulting from introducing the coordinate representation and choosing the correlation functions as the starting point is that one is able to calculate the half-widths and shifts with high accuracy, no matter how complicated the potential models are and no matter what kind of trajectories are chosen. In any case, the convergence of the calculated results is always guaranteed. As a result, with this new method, one can remove some uncertainties incorporated in the current width and shift studies. As a test, we present calculated Raman Q linewidths for the N_2–N_2 pair based on several trajectories, including the more accurate "exact" ones. Finally, by using this new method as a benchmark, we have carried out convergence checks for calculated values based on usual methods and have found that some results in the literature are not converged. [DOI: 10.1063/1.2139671]

I. INTRODUCTION

In order to carry out the forward modeling of atmospheric radiatiative transfer processes and to obtain information on the abundances of molecular species, temperature-pressure profiles, and other atmospheric properties, one needs accurate spectroscopic data. This includes not only line positions and strengths, but also the temperature-dependent Lorentzian half-widths and pressure shifts. Because the ambient atmospheric species, temperatures, and pressures are not always amenable to laboratory measurements, or because of the large number of transitions possible, one often has to rely on theoretical calculations. It is well known that the formalisms used to calculate half-widths and shifts of molecular spectral lines such as the Anderson-Tsao-Curnutte (ATC) theory,[1,2] the Bobert-Bonamy (RB) theory,[3,4] and others are based on two basic approximations: the binary collision and the impact approximations. With these two approximations, calculations of the pressure broadened half-widths and shifts of the absorber molecular lines are reduced to thermal averages of all possible collision processes involving a pair of molecules; and in comparison with the time of interest, these collisions are assumed to be completed instantaneously. In addition, both the ATC and RB formalism are semiclassical theories. In other words, the translational motion of the pair is treated classically, while their internal degrees of freedom are treated quantum mechanically. This semiclassical method is valid in calculating molecular spectral lines for temperatures of interest in atmospheric applications. However, the current theories are also based on other

[a)]Electronic mail: qma@giss.nasa.gov

assumptions. Some of these lack sound justification and could lead to uncertainties that affect the reliability of the calculated results. Thus, further refinements and improvements are necessary.

In this paper, we present a new theoretical formalism for the calculation of converged results for half-widths and shifts no matter how complicated the interaction potential is or what type of trajectory is used to describe the collisional path. This method is described in the next section and illustrated by calculations for the N_2-N_2 pair. In the final section, we discuss briefly the conclusions from the present study.

II. THEORY

A. Half-widths and shifts given by the perturbation expansion of the $\hat{S}$ matrix

The main computation task for calculating the Lorentzian half-widths and shifts is the evaluations of matrix elements appearing in the perturbation expansion of the $\hat{S}$ matrix ($=S_I \cdot S_F^*$, where S_I and S_F are scattering matrices in Hilbert space). Usually, in practice, these evaluations are limited to the second order of the expansion. For example, with the modified RB formalism,[5] the expressions of the half-widths and shifts are given by

$$\gamma = \frac{n_b}{2\pi c}\int_0^{+\infty} v f(v) dv \int_0^{+\infty} 2\pi b db \times [1 - \cos(S_1 + \mathrm{Im}\, S_2) e^{-\mathrm{Re}\, S_2}], \tag{1}$$

and

$$\delta = \frac{n_b}{2\pi c}\int_0^{+\infty} v f(v) dv \int_0^{+\infty} 2\pi b db \sin(S_1 + \mathrm{Im}\, S_2) e^{-\mathrm{Re}\, S_2}, \tag{2}$$

respectively, where $f(v)$ is the Maxwell-Boltzmann distribution function. In the above, S_1 and S_2 associated with the first and second orders of the perturbation expansion of the $\hat{S}$ matrix, respectively, are defined by

$$S_1 = \frac{1}{\hbar}\int_{-\infty}^{+\infty} dt \langle \mathcal{L}_1(t) \rangle \tag{3}$$

and

$$S_2 = \frac{1}{\hbar^2}\int_{-\infty}^{+\infty} dt \int_{-\infty}^{t} dt' \{\langle \mathcal{L}_1(t)\mathcal{L}_1(t') \rangle - \langle \mathcal{L}_1(t) \rangle \langle \mathcal{L}_1(t') \rangle\}, \tag{4}$$

where $\mathcal{L}_1(t)$ is a Liouville operator associated with the Hilbert interaction operator $\hat{V}(t)(\equiv e^{i(H_a+H_b)t/\hbar} V e^{-i(H_a+H_b)t/\hbar})$, and $\langle \cdots \rangle$ means an average over the internal degrees of the bath molecule carried out in the line space. As expected, evaluating S_2 is more difficult than S_1 and is outlined here. In order to calculate S_2, one has to rewrite everything in Eq. (4) back in terms of Hilbert operators and states. A comprehensive expression for S_2 is well known and can be found in the literature.[2–4] Usually, people prefer to represent S_2 by three terms labeled by $S_{2,\mathrm{outer},i}$, $S_{2,\mathrm{outer},f}$, and $S_{2,\mathrm{middle}}$, respectively. In the present study, we follow the same custom, and as an example we show how to calculate $S_{2,\mathrm{outer},i}$ in detail here. For simplicity, we assume both the absorber and bath molecules are linear.

It is well known that both the ATC and RB formalisms are applicable only for well-separated lines because they are based on the additional assumption that the Liouville operator $\hat{S}$ is diagonal in the line space of the absorber molecule. (That is, line coupling is neglected.) The purpose of introducing this assumption is to make the calculations more tractable. Now, we are ready to present the explicit expression for $S_{2,\mathrm{outer},i}$ which is given by

$$S_{2,\mathrm{outer},i} = \frac{1}{\hbar^2(2i+1)} \sum_{i_2} \rho_{i_2} \int_{-\infty}^{+\infty} dt \int_{-\infty}^{t} dt' \times \sum_{(m)} \langle i m_i i_2 m_{i_2} | \hat{V}(\boldsymbol{R}(t)) \hat{V}(\boldsymbol{R}(t')) | i m_i i_2 m_{i_2} \rangle, \tag{5}$$

where i and m_i represent initial states of the absorption line of interest, i_2 and m_{i2} the states of the bath molecule, ρ_{i2} is the density matrix of the bath molecule, and the symbol (m) means summations over all magnetic quantum numbers. In the above expression, $\boldsymbol{R}(t)$ is a vector connecting the two mass centers of the molecular pair. Thus, $\boldsymbol{R}(t)$, as a classical function of t, describes the translational motion of the molecular pair. With respect to the internal degrees and the translational degrees of the pair, the interaction potential V behaves differently: V is an operator acting on the former, while V depends on the latter parametrically. Based on this, one can write $S_{2,\mathrm{outer},i}$ in a form more suitable for calculations

$$S_{2,\mathrm{outer},i} = \frac{1}{\hbar^2(2i+1)} \sum_{i_2} \rho_{i_2} \sum_{i' i_2'} \sum_{(m)} \int_{-\infty}^{\infty} dt e^{i(\omega_{ii'} + \omega_{i_2 i_2'})t'} \times \langle i m_i i_2 m_{i_2} | V(\boldsymbol{R}(t)) | i' m_i' i_2' m_{i_2}' \rangle \times \int_{-\infty}^{t} dt' e^{-i(\omega_{ii'} + \omega_{i_2 i_2'})t'} \times \langle i' m_i' i_2' m_{i_2}' | V(\boldsymbol{R}(t')) | i m_i i_2 m_{i_2} \rangle, \tag{6}$$

where $\omega_{ii'} = (E_i^{(a)} - E_{i'}^{(a)})/\hbar$ and $\omega_{i_2 i_2'} = (E_{i_2}^{(b)} - E_{i_2'}^{(b)})/\hbar$. Then, once the potential model is chosen, one can use Eq. (6) as the starting point.

Usually, potential models consist of two parts representing the isotropic and anisotropic interactions, respectively. It is well known that the latter play a more crucial role than the former in phenomena induced by molecular interactions[6] and they are also more difficult to deal with. Therefore, we focus our attention on this part here. For simple potential models whose anisotropic part consists of the electrostatic interactions $V_{dd} + V_{dq} + V_{qd} + V_{qq} + \cdots$ only, the evaluation of $S_{2,\mathrm{outer},i}$, $S_{2,\mathrm{outer},f}$, and $S_{2,\mathrm{middle}}$ has been solved many years ago.

Because each of these electrostatic interaction components has distinguishable rotational symmetries, there are no couplings between two different components in calculating products of the two matrix elements of V in Eq. (6). In addition, there is no interweaving between the $\boldsymbol{R}(t)$ dependence and the internal degree dependence of these components, and the multipole-moment dependence can be factored out. As a result, one is able to introduce so-called "resonance functions" which are common for any $\boldsymbol{R}(t)$ and for any multipole-moment values. Although work related to the derivations of these resonance functions is tedious, especially for higher multipole interactions, the calculations are feasible and are only needed to be done once. Then, their "universal" nature enables one to easily obtain each of their contributions to $S_{2,\text{outer},i}$. Finally, by simply adding these results, one can get the total contribution to $S_{2,\text{outer},i}$.

B. Extension of the ATC and RB formalism applicable for complicated potentials

Given the fact that pressure broadening is a phenomenon induced by intermolecular interactions, it is not surprising that theoretical predictions of the half-widths and shifts depend sensitively on the potential models used in the calculations. In order to meet the accuracy requirements for these parameters needed for current atmospheric applications, it is necessary to choose more accurate potential models because a simple potential model consisting of the electrostatic interaction and an isotropic part is too crude to represent the complicated features of intermolecular interactions. A challenge arises when one adopts more realistic potential models, especially for those models containing a short-range interaction represented by an atom-atom model, such as the one given by

$$V_{\text{atom-atom}} = \sum_{i\in a}\sum_{j\in b} 4\epsilon_{ij}\left\{\frac{\sigma_{ij}^{12}}{r_{ij}^{12}} - \frac{\sigma_{ij}^{6}}{r_{ij}^{6}}\right\}, \tag{7}$$

where σ_{ij} and ϵ_{ij} are parameters and r_{ij} are distances between the ith atom of the absorber molecule a and the jth atom of the bath molecule b. In general, the atom-atom model can be expressed in terms of a spherical tensor expansion[7]

$$\begin{aligned} V_{\text{atom-atom}}(t) = &\sum_{l_1 l_2 l}\sum_{m_1 m_2 m}\sum_{n_{\{ij\}}}\sum_{wq}\frac{U(l_1 l_2 l, n_{\{ij\}}, wq)}{R^{l_1+l_2+q+2w}(t)} \\ &\times C(l_1 l_2 l, m_1 m_2 m) Y_{l_1 m_1}(\Omega_a) \\ &\times Y_{l_2 m_2}(\Omega_b) Y^*_{lm}(\Omega)(t), \end{aligned} \tag{8}$$

where $C(l_1 l_2 l, m_1 m_2 m)$ are the Clebsch-Gordan coefficients, $n_{\{ij\}}$ runs over all pairs of atom in Eq. (7), $q=6$ or 12, w is an integer index from 0 to infinity, and definitions for $U(l_1 l_2 l, n_{\{ij\}}, wq)$ can be found in the literature.[7] In the above expression, the translational motion is described by $R(t)$ and $\Omega(t)$ and orientations of the absorber and bath molecules are described by Ω_a and Ω_b, respectively. At this stage, a common practice is to follow the steps used in deriving the resonance functions for the electrostatic interaction. In order to maintain the universal nature of resonance functions, one has to deal with each individual term separately because different terms have different dependencies on $R(t)$ and $n_{\{ij\}}$. Then, as usual, albeit with some more tedious algebraic work, one can derive the matrix elements of $V_{\text{atom–atom}}$, insert these results obtained into Eq. (6), and separate the factors depending on t or t' from each other. Finally, one is able to obtain an expression for $S_{2,\text{outer},i}$ suitable for performing numerical calculations[8]

$$\begin{aligned} S_{2,\text{outer},i} = &\sum_{l_1 l_2}\sum_{i'}\sum_{i_2 i_2'}\sum_{n_{\{ij\}} n_{\{ij\}'}} D(l_1 l_2, n_{\{ij\}} n'_{\{ij\}}, i i' i_2 i_2') \\ &\times F_{l_1 l_2}^{n_{\{ij\}} n'_{\{ij\}}}(\omega_{ii'} + \omega_{i_2 i_2'}), \end{aligned} \tag{9}$$

where the D terms are reduced matrix elements and the F terms are the resonance functions defined by

$$\begin{aligned} F_{l_1 l_2}^{n_{\{ij\}} n'_{\{ij\}}}(\omega) = &\frac{1}{(2l_1+1)(2l_2+1)}\sum_{m_1 m_2}\sum_{lm}\sum_{wq}\sum_{l'm'}\sum_{w'q'} C(l_1 l_2 l, m_1 m_2 m) \\ &\times C(l_1 l_2 l', m_1 m_2 m) U(l_1 l_2 l, n_{\{ij\}}, wq) U(l_1 l_2 l', n'_{\{ij\}}, w'q') \\ &\times \int_{-\infty}^{\infty} dt e^{i\omega t}\frac{Y_{lm}(\Omega(t))}{R^{l_1+l_2+q+2w}(t)}\int_{-\infty}^{t} dt' e^{-i\omega t'}\frac{Y_{l'm'}(\Omega(t'))}{R^{l_1+l_2+q'+2w'}(t')}. \end{aligned} \tag{10}$$

In Eq. (10), the results of the two-dimensional integrations over t and t' are complex functions of ω. There are a lot of such functions because they are characterized by many summation indices, and for most models, some of these functions have to be evaluated numerically.

In practice, one has to introduce cutoffs to limit the number of terms in the expansions to be included in the calculations. A common practice is to introduce two cutoffs: one to set the limit for pairs of l_1 and l_2 to be considered, and the other to introduce the upper limit for the summation indices

w and w' in order to limit the highest inverse powers of $R(t)$ and $R(t')$ in Eq. (10). As shown by Eqs. (9) and (10) applicable for linear molecules, as one adopts higher cutoffs, the number of terms required to be evaluated increases dramatically. As a result, there could be a convergence problem in calculating contributions to $S_{2,\text{outer},i}$ using the atom-atom model, especially for cases where nonlinear molecules are involved because even more indices are required. It is worth mentioning that these two cutoffs have different characters because they are associated with the different nature of the summation indices. The first kind of cutoff deals with the irreducible tensor pairs of l_1 and l_2. Because there are no couplings between terms with different pairs of l_1 and l_2, it is certain that weak terms can only make small contributions to $S_{2,\text{outer},i}$. Therefore, a criterion for the convergence over this cutoff can be, more or less, reliably established. In contrast, with respect to the second kind of cutoff, there are couplings between terms ignored by the cutoff and terms considered with the same l_1 and l_2. We would like to emphasize here that the latter consists not only of the terms remaining in the spherical expansion of $V_{\text{atom-atom}}$, but also the electrostatic component labeled by l_1 and l_2. As a result, to ignore weak terms could cause significant errors because these could make significant contributions to $S_{2,\text{outer},i}$ through couplings with other, strong components. Therefore, it becomes more difficult to establish a reliable convergence criterion and, in addition, the convergence over this cutoff could become a formidable obstacle in practical calculations for molecular pairs unless the electrostatic interaction is overwhelmingly dominant.

Above, we have outlined the usual method for calculating $S_{2,\text{outer},i}$. A drawback of this method is that one could encounter trouble when atom-atom potential models are considered. In these cases, to adopt higher cutoffs in the spherical expansion and to consider all contributions including couplings between terms with the same categories of l_1 and l_2 whose origins could be one of any type (e.g., the long-range electrostatic, the long-range induction, the short-range atom-atom interactions, etc.) requires very much tedious work and many resonance functions such that one may not be able to obtain converged results.

The possibility of convergence failure forces one to wonder if this method is the best way to proceed. To seek a better way is one of the main motivations for the present study. Based on our experience in dealing with complicated potential models in treating far-wing line shapes and other problems, [9,10] we know that the coordinate representation used in those studies has advantages in dealing with complicated potentials because in this representation the potential operators are diagonal and can be treated as classical functions. As shown later in detail, with this powerful tool, one is able to obtain the converged results for any potential model, no matter how complicated these models are. In addition, all the potential coupling effects are automatically included in the calculations.

C. Irreducible tensors of the interaction in the perturbation expansion of the $\hat{S}$ matrix

With the standard method, the basis set in Hilbert space is constructed from $|im_i\rangle \otimes |i_2 m_{i2}\rangle$, the product of the states of two interacting molecules. On the other hand, instead of choosing the internal states, one can select the orientations of the pair of molecules as the basis set in Hilbert space; i.e., $|\delta(\Omega_a - \Omega_{a\alpha})\rangle \otimes |\delta(\Omega_b - \Omega_{b\alpha})\rangle$ where $\Omega_{a\alpha}$ and $\Omega_{b\alpha}$ represent orientations of the absorber and bath molecules specified by α, respectively. By introducing the coordinate representation, the potential becomes a diagonal operator and the matrix elements become multidimensional integrations.[9,10] As a result, one is able to rewrite $S_{2,\text{outer},i}$ as

$$
\begin{aligned}
S_{2,\text{outer},i} = {} & \frac{1}{\hbar^2(2i+1)} \sum_{i_2} \rho_{i_2} \int_{-\infty}^{\infty} dt \int_{-\infty}^{t} dt' \\
& \times \sum_{i' i_2'} \sum_{(m)} \int d\Omega_\alpha \int d\Omega_\beta e^{i(\omega_{ii'} + \omega_{i_2 i_2'})(t-t')} \\
& \times \langle im_i i_2 m_{i_2} | \alpha \rangle V_\alpha(\boldsymbol{R}(t)) \langle \alpha | i' m_i' i_2' m_{i_2}' \rangle \\
& \times \langle i' m_i' i_2' m_{i_2}' | \beta \rangle V_\beta(\boldsymbol{R}(t')) \langle \beta | im_i i_2 m_{i_2} \rangle, \qquad (11)
\end{aligned}
$$

where $|\alpha\rangle$ is a shorthand notation for the basis set in the coordinate representation of the molecular pair and the subscript α of V_α represents the potential evaluated at a specified orientation labeled by $\Omega_{a\alpha}$ and $\Omega_{b\alpha}$. The inner products $\langle im_i i_2 m_{i2} | \alpha \rangle$ represent a transformation between two basis sets of these two representations and are nothing but the well-known functions $Y^*_{im_i}(\theta_{a\alpha}\phi_{a\alpha}) \times Y^*_{i_2 m_{i_2}}(\theta_{b\alpha}\phi_{b\alpha})$. With some algebraic work, one is able to rewrite the above expression for $S_{2,\text{outer},i}$ in a more compact form

$$
\begin{aligned}
S_{2,\text{outer},i} = {} & \sum_{l_1 l_2} \int_{-\infty}^{\infty} \int_{-\infty}^{t} dt dt' G_{l_1 l_2}(t,t') \\
& \times W_{l_1}^{(a)}(t-t') W_{l_2}^{(b)}(t-t'). \qquad (12)
\end{aligned}
$$

In the above expression, two functions which are independent of the potential are defined by

$$
W_{l_1}^{(a)}(\tau) = \sum_{i'} (2i'+1) C^2(ii' l_1, 000) e^{i\omega_{ii'}\tau} \qquad (13)
$$

and

$$
W_{l_2}^{(b)}(\tau) = \sum_{i_2 i_2'} (2i_2+1)(2i_2'+1) \rho_{i_2} C^2(i_2 i_2' l_2, 000) e^{i\omega_{i_2 i_2'}\tau}, \qquad (14)
$$

respectively. Meanwhile, the functions $G_{l_1 l_2}(t,t')$ introduced above are defined by

$$G_{l_1 l_2}(t,t') = \frac{\hbar^{-2}}{16\pi^2(2l_1+1)(2l_2+1)} \sum_{m_1 m_2} \int d\Omega_\alpha \times Y^*_{l_1 m_1}(\theta_{a\alpha}\phi_{a\alpha}) Y^*_{l_2 m_2}(\theta_{b\alpha}\phi_{b\alpha}) V_\alpha(\boldsymbol{R}(t)) \times \int d\Omega_\beta Y_{l_1 m_1}(\theta_{a\beta}\phi_{a\beta}) Y_{l_2 m_2}(\theta_{b\beta}\phi_{b\beta}) V_\beta(\boldsymbol{R}(t')). \tag{15}$$

In general, one can express $V_\alpha(\boldsymbol{R}(t))$ in terms of the standard spherical expansions as

$$V_\alpha(\boldsymbol{R}(t)) = \sum_{l_1 l_2 l} A(l_1 l_2 l; R(t)) \times \sum_{m_1 m_2 m} C(l_1 l_2 l, m_1 m_2 m) \times Y_{l_1 m_1}(\Omega_{a\alpha}) Y_{l_2 m_2}(\Omega_{b\alpha}) Y^*_{lm}(\Omega(t)). \tag{16}$$

It is worth mentioning that both $R(t)$ and $\Omega(t)$ depend on the velocity and trajectories along which the translational motion moves. In comparison with Eq. (8), terms with the same summation indices l_1, l_2, and l have been grouped together in Eq. (16). By inserting these expressions for $V_\alpha(\boldsymbol{R}(t))$ and $V_\beta(\boldsymbol{R}(t'))$ into Eq. (15), one can carry out the integrations over Ω_α and Ω_β analytically based on the normalization and orthogonality of the spherical harmonics associated with each of the two molecules and obtain an expression for performing numerical calculations,

$$G_{l_1 l_2}(t,t') = \frac{\hbar^{-2}}{(4\pi)^3(2l_1+1)(2l_2+1)} \times \sum_l (-1)^{(l_1+l_2+l)}(2l+1) P_l(\cos\Theta_{t,t'}) \times A(l_1 l_2 l; R(t)) A(l_1 l_2 l; R(t')), \tag{17}$$

where $\Theta_{t,t'}$ are angles between two vectors $\boldsymbol{R}(t)$ and $\boldsymbol{R}(t')$. As shown by Eq. (17), if one knows how $\boldsymbol{R}(t)$ varies with the time, to calculate values of $G_{l_1 l_2}(t,t')$ is straightforward. In order to proceed, one needs to know the velocity and the trajectory.

As shown above, $G_{l_1 l_2}(t,t')$ arise directly from introducing the coordinate representation. They are the keystone of the present formalism and play a crucial role in calculating $S_{2,\text{outer},i}$. In fact, the primary advantages of the new method are associated with them. First of all, because the potentials are ordinary functions in the coordinate representation, no matter how complicated they are, to evaluate their values is easy. As a result, one can freely choose more realistic potential models, and one does not need to worry about the cutoffs any more because this convergence obstacle has been obviated. This is the most important advantage. With the usual method, as explained above, the second kind of cutoff could cause convergence trouble because as the cutoff increases, the number of the resonance functions required to be evaluated increases dramatically. In contrast, with the present method, this does not happen in calculating $G_{l_1 l_2}(t,t')$. The second kind of cutoff affects only how accurately one needs to evaluate the coefficients $A(l_1 l_2 l; R(t))$ and $A(l_1 l_2 l; R(t'))$ in Eq. (17). No matter how high the cutoff goes in calculating these coefficients, there are small differences as measured by the needed computational resources. As a result, in evaluating $A(l_1 l_2 l; R(t))$ and $A(l_1 l_2 l; R(t'))$ we can use a cutoff which is sufficiently high to guarantee convergence. Second, with the new method, one can select more accurate trajectories. The reason is that no matter which model is chosen, after the trajectories become available, there are no significant differences in evaluating $G_{l_1 l_2}(t,t')$. The only thing that matters is how easy it is to find the trajectories from the initial collision conditions. Fortunately, within the current approximation level in which one assumes that the trajectory is governed by the isotropic potential, to derive trajectories with specified impact parameter b is a two-body central force problem that is well solved in classical mechanics. As shown later, we are able to handle this problem readily. Therefore, one can conclude that the present method can easily be extended to consider more accurate trajectory models than the parabolic trajectory widely used in previous calculations. Third, because $A(l_1 l_2 l; R(t))$ and $A(l_1 l_2 l; R(t'))$ are the entire components of $V(\boldsymbol{R}(t))$ and $V(\boldsymbol{R}(t'))$, one does not need to worry about missing any couplings since these are fully taken into account automatically. This is another big advantage over the usual method.

Furthermore, the well-behaved profile of $G_{l_1 l_2}(t,t')$ itself facilitates the development of the present formalism. Unlike the wildly oscillating features appearing in the resonance functions within the usual method, $G_{l_1 l_2}(t,t')$ do not exhibit these and are well-behaved smooth functions. These features are important in practical calculations because further mathematical manipulations of $G_{l_1 l_2}(t,t')$ are necessary and high accuracy can be preserved in these steps. In addition, if one sets $t=0$ when the translational motion reaches the closest distance r_c along the trajectory, the magnitudes of $G_{l_1 l_2}(t,t')$ decrease very quickly to zero as $|t|$ and/or $|t'|$ increase. This rapid decrease in magnitude will play a crucial role later to guarantee that the autocorrelation functions derived from them maintain this same feature. In summary, to calculate $G_{l_1 l_2}(t,t')$ is so straightforward that some approximations (i.e., the second kind of cutoff and the parabolic trajectory) currently introduced can be completely avoided. As a result, we expect that the corresponding calculated results would be more physically realistic.

Before we complete our discussions of $G_{l_1 l_2}(t,t')$, we would like to explain the physical meanings of their labels and arguments. Because they result from the second-order

expansion of the $\hat{S}$ matrix, they have two labels and two arguments. It is not surprising that there is no unnecessary geometric dependence remaining because averages over the magnetic quantum numbers m_1 and m_2 have been carried out. The two discrete labels l_1 and l_2 of $G_{l_1 l_2}(t,t')$ represent the ranks of the irreducible tensors constructed by a product of two potentials. Meanwhile, the two continuous arguments t and t' represent positions of these two potentials in the time development process of the $\hat{S}$ matrix. The discrete and continuous natures of the labels and arguments of $G_{l_1 l_2}(t,t')$ correspond to the quantum and classical natures by which the internal degrees and the translational motion are treated in the formalism.

For later convenience, by changing integration variables in Eq. (12), one is able to express $S_{2,\text{outer},i}$ as

$$S_{2,\text{outer},i} = \sum_{l_1 l_2} \int_{-\infty}^{\infty} \int_{0}^{\infty} dt dt' G_{l_1 l_2}(t, t-t') W_{l_1}^{(a)}(t') W_{l_2}^{(b)}(t')$$
$$= \sum_{l_1 l_2} \int_{0}^{\infty} dt W_{l_1}^{(a)}(t) W_{l_2}^{(b)}(t) \times \int_{-\infty}^{\infty} dt' G_{l_1 l_2}(t' + t/2, t' - t/2). \quad (18)$$

Although, it is $G_{l_1 l_2}(t'+t/2, t'-t/2)$, not $G_{l_1 l_2}(t,t')$ that are required in actual calculations, it is obvious that all the discussion above concerning the latter is also applicable for the former.

D. Irreducible autocorrelation functions of the interaction

The functions $G_{l_1 l_2}(t'+t/2, t'-t/2)$ contain all raw information on the dynamical development process of the $\hat{S}$ matrix. As shown by Eq. (18), they appear as a convolution integration. This implies that $G_{l_1 l_2}(t'+t/2, t'-t/2)$ can be condensed to simpler functions which contain the core information. The latter are nothing but the autocorrelation functions representing the net dynamical effect from overlaps between $V(\boldsymbol{R}(t))$ and $V(\boldsymbol{R}(t'))$ in the second order of the perturbation expansion of $\hat{S}$ and can be defined as

$$F_{l_1 l_2}(t) = \int_{-\infty}^{\infty} dt' G_{l_1 l_2}(t' + t/2, t' - t/2). \quad (19)$$

In the present formalism the internal degrees of the molecular pair have been treated fully quantum mechanically. However, by introducing the coordinate representation, in the expressions for $G_{l_1 l_2}(t,t')$ shown by Eq. (15), one can freely interchange the order of the potentials $V_\alpha(\boldsymbol{R}(t))$ and $V_\beta(\boldsymbol{R}(t'))$ because they are ordinary functions. As a result, the correlation functions $F_{l_1 l_2}(t)$ introduced above look like the classical ones and are real, even functions. Because $G_{l_1 l_2}(t'+t/2, t'-t/2)$ are well-behaved functions and their values go to zero very quickly as $|t'|$ increases, one does not face any difficulty in performing the integration in Eq. (19) numerically and maintaining high accuracy. In our calculations, we reduce the range of integration from infinity to a finite value such that the magnitudes of the integrand fall down by at least six orders of magnitude. Then, with DQDAG, an integration subroutine using a globally adaptive scheme based on Gauss-Kronrod rules in IMSL, we can easily get highly accurate values of $F_{l_1 l_2}(t)$ for any t of interest. In summary, these autocorrelation functions are the core of the present formalism containing all the physics necessary in calculating widths and shifts. They are well-behaved functions and their values can be easily derived with a high accuracy. However, it turns out that within the impact theory, it is more useful to transform this physical information given in the time domain into the frequency domain. The next section is devoted to this subject.

E. Fourier transforms of the autocorrelation functions and their Cauchy principal integrations

After the correlation functions are available, the next step is to find their corresponding Fourier transforms $H_{l_1 l_2}(\omega)$ defined by

$$H_{l_1 l_2}(\omega) = \frac{1}{\sqrt{2\pi}} \int_{-\infty}^{\infty} dt e^{i\omega t} F_{l_1 l_2}(t). \quad (20)$$

At this stage, it looks like we may face a difficulty in handling the infinite integrations whose integrands could oscillate wildly. Fortunately, one can avoid these integrations completely and obtain the Fourier transforms $H_{l_1 l_2}(\omega)$ easily and accurately. The key point here is to exploit the profile of $F_{l_1 l_2}(t)$. Because the argument t of $F_{l_1 l_2}(t)$ is a measurement of how far apart the two potentials are, their magnitudes decrease very quickly as $|t|$ increases. This enables one to assume their time range is not $[-\infty, \infty]$, but $[-T, T]$ where T is a finite value. In our calculations, we choose T such that the magnitudes of $F_{l_1 l_2}(t)$ have decreased at $t=T$ (or $t=-T$) by seven orders of magnitude from their values at $t=0$. As an example, for a typical collision path of the N_2–N_2 pair at 296 K, T is around 7.4 ps. Thus, to limit the interval to $[-T, T]$ is well within the uncertainty tolerance in the calculations. Because $F_{l_1 l_2}(t)$ are time-limited, well-behaved functions, it becomes more certain that their continuous Fourier transforms $H_{l_1 l_2}(\omega)$ are band-limited functions of ω.[11] As a result, one is able to represent these continuous Fourier transforms by discrete Fourier transforms which can easily be computed.[11] As shown later in Fig. 7, these Fourier transform functions do decrease very quickly as ω increases. In summary, $H_{l_1 l_2}(\omega)$ can easily be derived with high accuracy.

Finally, for later usage, we introduce $I_{l_1 l_2}(\omega)$, the Cauchy principal integrations of $H_{l_1 l_2}(\omega)$, obtained from the following expression:

$$I_{l_1 l_2}(\omega) = -\frac{1}{\pi} P \int_{-\infty}^{\infty} d\omega' \frac{1}{\omega' - \omega} H_{l_1 l_2}(\omega'), \tag{21}$$

where P means the principal part. After $H_{l_1 l_2}(\omega)$ become available, one can calculate these functions $I_{l_1 l_2}(\omega)$ with appropriate subroutines (for example, DQAWC, an adaptive integration for Cauchy principal values, in IMSL). We note that the relationship between $H_{l_1 l_2}(\omega)$ and $I_{l_1 l_2}(\omega)$ is governed by the Hilbert transforms.[12]

Now, except for discussion about the trajectories, we have completed most of the work and are one step away from attaining the final results. With Eqs. (18)–(20), one is able to express $S_{2,\text{outer},i}$ as

$$\begin{aligned} S_{2,\text{outer},i} &= \frac{1}{\sqrt{2\pi}} \sum_{l_1 l_2} \int_0^{\infty} dt W_{l_1}^{(a)}(t) W_{l_2}^{(b)}(t) \int_{-\infty}^{\infty} d\omega e^{-i\omega t} H_{l_1 l_2}(\omega) \\ &= \frac{1}{\sqrt{2\pi}} \sum_{l_1 l_2} \int_{-\infty}^{\infty} d\omega H_{l_1 l_2}(\omega) \int_0^{\infty} dt e^{-i\omega t} W_{l_1}^{(a)}(t) W_{l_2}^{(b)}(t). \end{aligned} \tag{22}$$

Furthermore, with Eqs. (13) and (14), one can obtain

$$\begin{aligned} S_{2,\text{outer},i} &= \frac{1}{\sqrt{2\pi}} \sum_{l_1 l_2} \left\{ \sum_{i'} (2i'+1) C^2(ii' l_1, 000) \sum_{i_2 i_2'} (2i_2+1)(2i_2'+1) \rho_{i_2} C^2(i_2 i_2' l_2, 000) \int_{-\infty}^{\infty} d\omega H_{l_1 l_2}(\omega) \int_0^{\infty} dt e^{-i(\omega - \omega_{ii'} - \omega_{i_2 i_2'})t} \right\} \\ &= \frac{1}{\sqrt{2\pi}} \sum_{l_1 l_2} \left\{ \sum_{i'} (2i'+1) C^2(ii' l_1, 000) \sum_{i_2 i_2'} (2i_2+1)(2i_2'+1) \rho_{i_2} C^2(i_2 i_2' l_2, 000) \int_{-\infty}^{\infty} d\omega H_{l_1 l_2}(\omega) \left[\pi \delta(\omega - \omega_{ii'} - \omega_{i_2 i_2'}) \right.\right. \\ &\quad \left.\left. - iP \frac{1}{\omega - \omega_{ii'} - \omega_{i_2 i_2'}} \right] \right\}. \end{aligned} \tag{23}$$

With the above expression, one can easily obtain $\text{Re}(S_{2,\text{outer},i})$

$$\begin{aligned} \text{Re}(S_{2,\text{outer},i}) = \sqrt{\frac{\pi}{2}} \sum_{l_1 l_2} \Bigg\{ & \sum_{i'} (2i'+1) C^2(ii' l_1, 000) \\ & \times \sum_{i_2 i_2'} (2i_2+1)(2i_2'+1) \rho_{i_2} \\ & \times C^2(i_2 i_2' l_2, 000) H_{l_1 l_2}(\omega_{ii'} - \omega_{i_2 i_2'}) \Bigg\}, \end{aligned} \tag{24}$$

and $\text{Im}(S_{2,\text{outer},i})$

$$\begin{aligned} \text{Im}(S_{2,\text{outer},i}) = \sqrt{\frac{\pi}{2}} \sum_{l_1 l_2} \Bigg\{ & \sum_{i'} (2i'+1) C^2(ii' l_1, 000) \\ & \times \sum_{i_1 i_2} (2i_2+1)(2i_2'+1) \rho_{i_2} \\ & \times C^2(i_2 i_2' l_2, 000) I_{l_1 l_2}(\omega_{ii'} - \omega_{i_2 i_2'}) \Bigg\}. \end{aligned} \tag{25}$$

As shown by Eqs. (24) and (25), after $H_{l_1 l_2}(\omega)$ and $I_{l_1 l_2}(\omega)$ are available, to calculate $\text{Re}(S_{2,\text{outer},i})$ and $\text{Im}(S_{2,\text{outer},i})$ is straightforward; the only thing needed to do is to pick up values of $H_{l_1 l_2}(\omega)$ and $I_{l_1 l_2}(\omega)$ accordingly and to add the results together.

Similarly, we can derive expressions for $S_{2,\text{outer},f}$ and $S_{2,\text{middle}}$ in terms of $H_{l_1 l_2}(\omega)$ and/or $I_{l_1 l_2}(\omega)$. In fact, expressions for $\text{Re}(S_{2,\text{outer},f})$ and $\text{Im}(S_{2,\text{outer},f})$ are the same as Eqs. (23) and (24) for $\text{Re}(S_{2,\text{outer},i})$ and $\text{Im}(S_{2,\text{outer},i})$, except for the replacement of the initial quantum number i by the final one j. Meanwhile, $S_{2,\text{middle}}$, which is real, is given by

$$\begin{aligned} S_{2,\text{middle}} = (-1)^{J+1} \sqrt{2\pi} \sum_{l_1 l_2} & (2i+1)(2j+1) \\ & \times (-1)^{l_1} C(iil_1, 000) C(jjl_1, 000) \\ & \times W(ijij, Jl_1) \sum_{i_1 i_2'} (2i_2+1)(2i_2'+1) \rho_{i_2} \\ & \times C^2(i_2 i_2' l_2, 000) H_{l_1 l_2}(\omega_{i_2 i_2'}), \end{aligned} \tag{26}$$

where $W(ijij, Jl_1)$ are the Racah coefficients. In the above expression, J is the rank of the transition operator. For example, $J=0$ for isotropic Raman transitions, $J=1$ for electric dipole transitions, $J=2$ for anisotropic Raman transitions, and so on.

F. Trajectories

Before proceeding, we first note that all of the correlation functions, Fourier transforms, and Cauchy integration functions depend on the velocity v and the trajectory labeled by r_c. Therefore, one has to keep in mind that there are always two parameters, v and r_c, attached to these functions. Now, we would like to show briefly how within the new formalism one can easily perform the linewidth and shift calculations based on more accurate trajectories than the straight line and the parabolic trajectories commonly used in the usual method. Before beginning, we reiterate that our work is still based on the basic assumption that the trajectory

is governed by the isotropic potential only; i.e., the anisotropic interaction does not play any role in determining the trajectory along which the two interacting molecules move in the collisional process. Of course, this is not true and this limitation is a big drawback suffered by most of theoretical width and shift calculations, except for a few done by Green, based on close-coupling scattering theory applicable only for simple systems usually consisting of one atom and one molecule.[13]

Since Robert and Bonamy developed the BR formalism, there are two trajectories[3] which are commonly used in calculations. We label them as the "parabolic" and the modified parabolic trajectories here. The first one assumes the trajectory is still a straight path, but the modulus $R(t)$ is given by $R(t)=\sqrt{r_c^2+v_c'^2t^2}$. This implies that the translation motion moves with an "apparent" velocity defined by $v_c'=v_0\{1+8\epsilon/mv^2[5(\sigma/r_c)^{1/2}-2(\sigma/r_c)^6]\}^{1/2}$. The second one is a modified version in which the straight line is replaced by a curve defined by $\sin\theta(t)\approx v_c t/\sqrt{r_c^2+v_c'^2t^2}$ and $\cos\theta(t)=\sqrt{1-\sin^2\theta(t)}$ where $v_c(=v\{1-8\epsilon/mv^2[(\sigma/r_c)^{12}-(\sigma/r_c)^6]\}^{1/2})$ is the velocity at $R=r_c$. However, it seems that one cannot make this replacement everywhere because $\sin\theta(t)$ could be larger than 1 as t increases for some trajectories in which $v_c>v_c'$. This implies that one has to manipulate it further, more or less, arbitrarily.

More recently, there have been attempts by Buldyreva *et al.* to consider the "exact" trajectory.[14,15] Their work is based on Bykov's method presented more than a decade ago, but no computation of linewidths was performed at that time.[16] A basic idea of Bykov is that by changing the integration variable from the time t to the distance r in calculating the resonance functions, the trajectory dependence of the resonance functions can be explicitly taken into account. There are two kinds of the "exact" trajectories considered according to which part of the potential is used to determine the trajectory: an extra LJ model or the isotropic part of the potential itself. Of course, the latter is more reasonable than the former.

We now show how to deal with this problem. We think that in comparison with Bykov's method, the present one is simpler and more straightforward. As shown by Eq. (17), when one calculates $G_{l_1l_2}(t,t')$ [or $G_{l_1l_2}(t'+t/2,t'-t/2)$], one needs to know how $\boldsymbol{R}(t)$ changes along the trajectory. Therefore, taking into account the trajectory dependence is more natural here. In addition, after the trajectories are available and one knows how the relative motion moves along them, there are no differences between the straight line, the parabolic, and the "exact" trajectories. As a result, the only thing required is to show how to find the "exact" trajectory. As an example, we show here how to deal with the more difficult one, i.e., the "exact" trajectory determined by the exact isotropic part of the interaction.

In the present study, the trajectories are labeled by the closest distance r_c. We assume that the trajectory lies in the XOY plane and it is described by $R(t)$ and $\theta(t)$. Based on energy E and angular momentum L conservation, the trajectory of interest is determined by the following two equations:[17]

$$t=\int_{r_c}^{R}\frac{1}{\sqrt{\frac{2}{m}(E-V_{\mathrm{iso}}(r))-\frac{L^2}{m^2r^2}}}dr$$
$$=\frac{r_c}{v}\int_1^{R/r_c}\frac{ydy}{\sqrt{y^2-1+\frac{2V_{\mathrm{iso}}(r_c)}{mv^2}-y^2\frac{2V_{\mathrm{iso}}(r_cy)}{mv^2}}} \quad (27)$$

and

$$\theta=\int_{r_c}^{R}\frac{L}{mr^2\sqrt{\frac{2}{m}(E-V_{\mathrm{iso}}(r))-\frac{L^2}{m^2r^2}}}dr$$
$$=\sqrt{1-\frac{2V_{\mathrm{iso}}(r_c)}{mv^2}}\times\int_1^{R/r_c}\frac{dy}{y\sqrt{y^2-1+\frac{2V_{\mathrm{iso}}(r_c)}{mv^2}-y^2\frac{2V_{\mathrm{iso}}(yr_c)}{mv^2}}}, \quad (28)$$

where $V_{\mathrm{iso}}(r)=(4\pi)^{-3/2}A(000;r)$. With the subroutine DQDAG to carry out the above integrations for different values of R/r_c from $t=0$ to $t=1.5$ T, one is able to obtain two functions $t(R)$ and $\theta(R)$ necessary to determine the trajectory. Then, with a reverse procedure, one can obtain $R(t)$ and $\theta(t)$ for $0\leqslant t\leqslant 1.5$ T. Due to the symmetry of $R(-t)=R(t)$ and $\theta(-t)=-\theta(t)$, we can obtain the whole trajectory. According to our tests, if one chooses about 400 points to depict the whole trajectory with more points around $R=r_c$ and fewer points elsewhere, the job requires less than 40 s of CPU time. We expect that this resolution is fine enough to depict the trajectories well, even those with r_c close to the minimum where the bending is largest. Therefore, one can conclude that with our new method, to consider this kind of "exact" trajectory does not add a big burden to the computational effort.

As an example, we consider these four trajectories at $T=296$ K derived for a molecular pair of N_2–N_2. The potential model used here is from a paper by Looney and Rosasco.[18] The parameters of $V_{\text{atom-atom}}$ given in these authors' notation are $\epsilon_{\alpha\beta}=36.4$ K and $\sigma_{\alpha\beta}=3.20$ Å. Meanwhile, the Lennard-Jones (LJ) parameters are $\epsilon=95.2$ K and $\sigma=3.75$ Å, and the quadrupole moment of N_2 is -1.30 D Å. In Fig. 1, we plot trajectories occurring near to a head-on collision by selecting $r_c=3.50$ Å. Because the repulsive force is dominant (except for the straight path) all three other trajectories bend away from the scattering center (at the origin of the plane). The two parabolic ones are represented by the dash-dotted and dashed lines, respectively. The two "exact" ones are given by a dotted and a solid curve, respectively. In addition, by adding small circles on the curves, we explicitly show how fast the relative motion of the pair moves along the trajectories. A travel time from one circle to its next is 0.005 ps. To show this feature is important because one has to rely on both this and the trajectory to know how $\boldsymbol{R}(t)$ varies with time; besides the anisotropic interaction, the latter is needed in calculating $G_{l_1l_2}(t'+t/2,t'-t/2)$ as shown by Eq. (17). It is worth noting that the relative motion moves

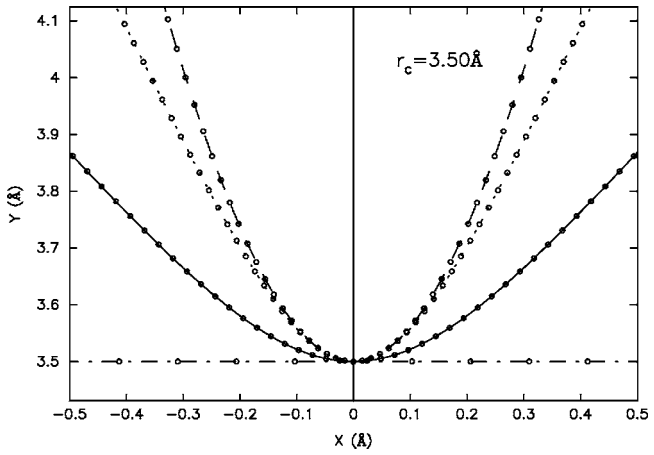

FIG. 1. Calculated trajectories for a molecular pair of N_2-N_2 at 296 K with $r_c=3.50$ Å. The scattering center is at the origin of the XY plane. The two "exact" trajectories determined by $V_{\rm iso}(R)$ and $V_{\rm LJ}(R)$ are represented by the solid and dotted lines, respectively. The two "parabolic" trajectories are given by the dot-dashed and dashed lines. Small circles are added on the trajectories such that a travel time between circles is 0.005 ps.

with the highest speed along the first "parabolic" path. The higher "apparent" velocity v_c' applicable in the straight path is required to compensate for the bending effect in other trajectories such that the increase of the modulus $R(t)$ can, more or less, keep a similar pace with the others. In Fig. 2, we present these trajectories with $r_c=4.50$ Å at which the attractive force is dominant. Because a larger scale is used, a travel time from one circle to its next is 0.05 ps.

As shown by the figure, except for the straight path, all others bend towards the scattering center. As a result, the "apparent" velocity v_c' with which the relative motion moves along the first trajectory becomes the smallest. As shown in these two figures, there are significant differences between two "exact" trajectories, especially for the head-on collision with $r_c=3.50$ Å. This is one indication that different choices of the LJ parameters could significantly affect the calculated line widths and shifts.

Furthermore, instead of the impact parameter b, most people prefer to use the closest distance r_c to label the trajectory. Accordingly, the integration variable is changed from

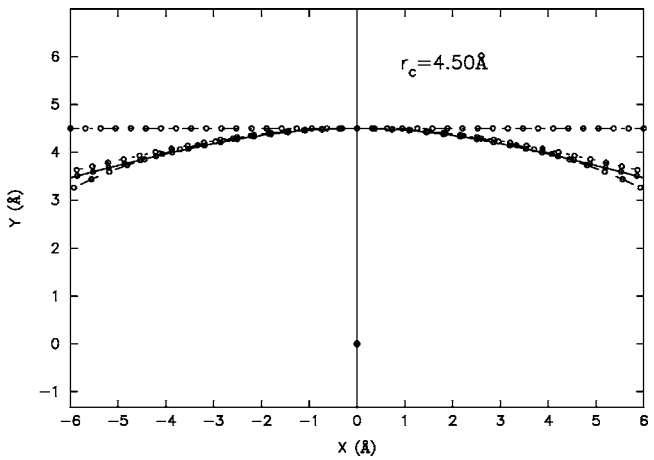

FIG. 2. The same as Fig. 1 except for $r_c=4.50$ Å and a travel time between circles is 0.005 ps.

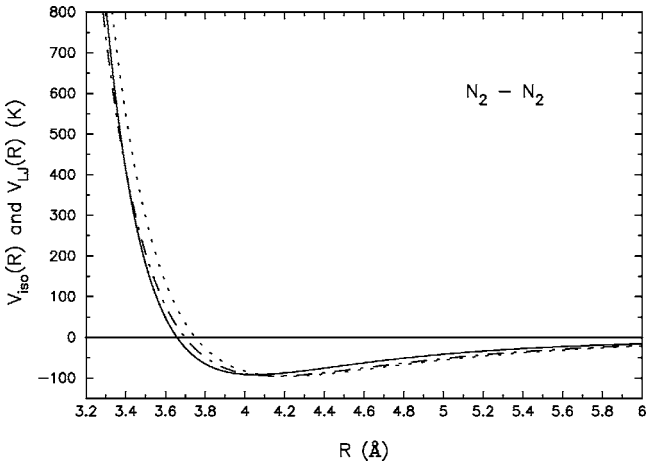

FIG. 3. The profiles of $V_{\rm iso}(R)$ and $V_{\rm LJ}(R)$. The solid line is for $V_{\rm iso}(R)$. The dotted line is the LJ model $V_{\rm LJ}(R)$ with $\epsilon=95.2$ K and $\sigma=3.75$ Å. A better LJ model with $\epsilon=95.05$ K and $\sigma=3.698$ Å is given by a dot-dashed line.

b to r_c and the lower limit from 0 to $r_{c,\min}$ in Eqs. (1) and (2). The latter can be derived from the expression directly

$$r_{c,\min}=\sigma\frac{2^{1/6}}{\left(1+\sqrt{1+\frac{mv^2}{2\epsilon}}\right)^{1/6}}, \tag{29}$$

where σ and ϵ are the LJ parameters, for the two parabolic trajectories and the "exact" one governed by the LJ model. Meanwhile, for the "exact" trajectory governed by $V_{\rm iso}(R)$, the value of $r_{c,\min}$ can be derived numerically from the equation

$$\frac{2V_{\rm iso}(r_{c,\min})}{mv^2}-1=0. \tag{30}$$

Based on the potential model used here, we find that values of $r_{c,\min}$ is 3.4626 Å from Eq. (29) and 3.4124 Å from Eq. (30). Although the difference between these two values looks small, it could affect calculated linewidths and shifts significantly for cases where the integrands enhance quickly as r_c approaches $r_{c,\min}$ in Eqs. (1) and (2). In order to show the problem more clearly, we present the exact $V_{\rm iso}(R)$ interaction and a LJ model $V_{\rm LJ}(R)$ with $\epsilon=95.2$ K and $\sigma=3.75$ Å in Fig. 3. As shown by the figure, the latter does not match the former well. Instead, if one simply adopts the values of ϵ and σ listed in the literature[19] (i.e., $\epsilon=95.05$ K and $\sigma=3.698$ Å), a much better fitting can be obtained.

We think that significant uncertainties can be introduced by using a LJ potential with freely adjustable parameters unless the selected LJ model matches $V_{\rm iso}(R)$ well. In reality, the physics is such that it is the anisotropic interaction, not the isotropic interaction that plays the major role in molecular line broadening. If calculated the results depend more sensitively on the latter, they become less physically meaningful no matter how good they appear to be. We will discuss this topic further later.

G. Profiles of $G_{l_1l_2}(z'+z/2,z'-z/2)$ and $F_{l_1l_2}(z)$

In this section, we show some examples of $G_{l_1l_2}(t'+t/2,t'-t/2)$ and $F_{l_1l_2}(t)$. We prefer to change the time vari-

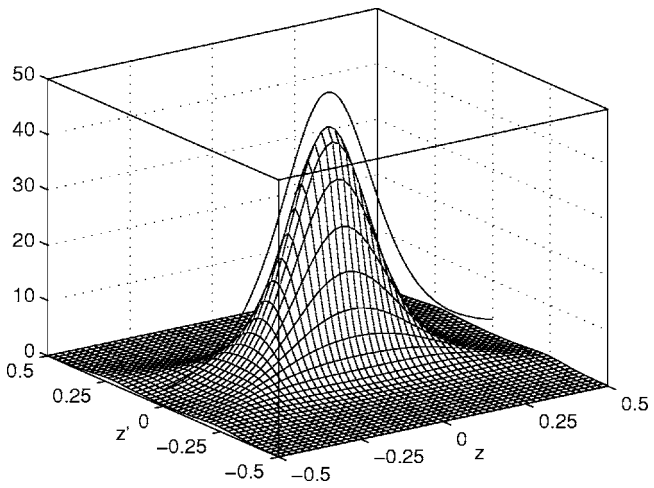

FIG. 4. Calculated function $G_{22}(z'+z/2,z'-z/2)$ (in ps^{-2}) at 296 K for a molecular pair of N_2-N_2. The calculation is based on the "exact" trajectory with $r_c=3.50$ Å determined by $V_{iso}(R)$. The corresponding correlation function $F_{22}(z)$ at 3.50 Å is also plotted by a single line in the figure.

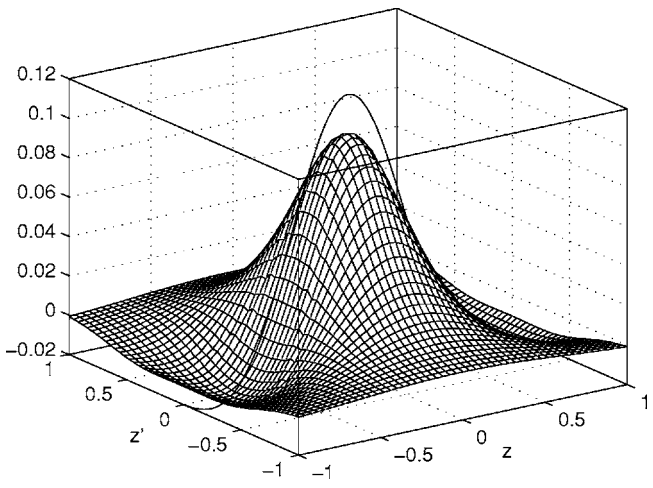

FIG. 5. The same as Fig. 4, except for $r_c=4.50$ Å.

able t to a dimensionless variable z defined by $z\equiv vt/r_c$ for the "exact" trajectories or defined by $z\equiv v_c't/r_c$ for the parabolic ones. Accordingly, we change the frequency variable ω to a dimensionless k defined by $k\equiv r_c\omega/v$ or $k\equiv r_c\omega/v_c'$ later. For simplicity, in the following we use the same notations for these new functions. We again choose N_2-N_2 as an example because this system has been studied by many researchers and we adopt the potential model used in plotting the trajectories. With respect to the irreducible tensor ranks of l_1 and l_2, we only present results for the major pair of $l_1=2$ and $l_2=2$. Meanwhile, as mentioned above, there are no big differences in dealing with the different model trajectories. In fact, we have made tests for all the trajectories discussed above; however, we present only results based on the "exact" trajectory determined by $V_{iso}(R)$.

In the present study, we will not perform an average over velocities. Instead, we replace all velocities by the mean thermal velocity ($v=\sqrt{8kT/\pi m}$). As a result, we have removed the velocity dependences from all functions. However, besides their explicit variables such as z and z', they still depend on the trajectory parameter r_c. Therefore, in general, one has to use contour plots. Finally, it is worth mentioning that except for the last two figures (Figs. 10 and 11) in order to show that the convergence problem exists in the literature, we are sure that all our calculated results in the following figures are converged. In Figs. 4 and 5, we show profiles of $G_{22}(z'+z/2,z'-z/2)$ at two selected r_c values. In Fig. 4, we present this function evaluated from an almost head-on "strong" collision with $r_c=3.50$ Å. As shown in the figure, there is a very sharp peak located at $z=0$ and $z'=0$, and the magnitude decreases very quickly as $|z|$ and/or $|z'|$ increase. In Fig. 5, we present the results obtained from a "mild" collision with $r_c=4.50$ Å. By comparing these two figures, we find that the magnitudes decrease dramatically from a strong collision to a mild collision. Meanwhile, the latter's profile contains more features than the former and the decrease in magnitude is slower. As a result, the scales for the z and z' axes used in Fig. 5 have been doubled. In addition, symmetries of $G_{l_1l_2}(z'+z/2,z'-z/2)$ for $z\rightarrow -z$, for $z'\rightarrow -z'$, and interchanging both z and z' (i.e., $z\rightarrow -z$ and $z'\rightarrow -z'$) are clearly shown in these figures. The last symmetry results directly from the fact that collision processes are time-reversal invariant. In order to show the correlation functions derived directly from these G functions, we have also plotted the function $F_{22}(z)$ using a single line in the figures. However, in order to fit the scales in these plots, the magnitudes of $F_{22}(z)$ have been adjusted. Therefore, one should only focus on their patterns, not their magnitudes.

The autocorrelation functions plotted in Figs. 4 and 5 are not adequate to show how they vary with z and r_c. Therefore, a contour plot is necessary. With Eq. (19), we derive the autocorrelation function with $l_1=2$ and $l_2=2$ and present the results for $z\geqslant 0$ and 3.5 Å$\leqslant r_c\leqslant$8.0 Å in Fig. 6. Because $F_{22}(z)$ is an even function, it is unnecessary to plot it with $z<0$. With respect to the range of r_c, we intentionally start the plot from 3.5 Å, not $r_{c,\min}$ because we want to avoid a high peak there. Otherwise, a much larger scale would be necessary which would not show the whole profile well. Why we selected 8.0 Å as the upper limit will become clear

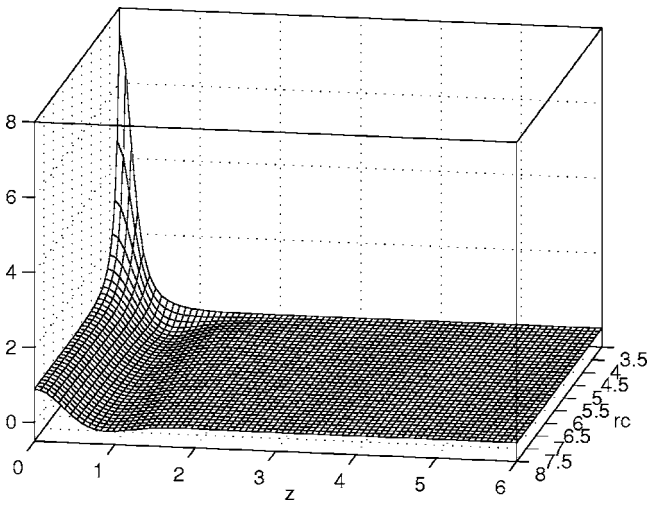

FIG. 6. Autocorrelation function $F_{22}(z)$ (in ps^{-2}) at 296 K for a molecular pair of N_2-N_2 as a two-dimensional function of z (dimensionless) and r_c (in angstrom). By multiplying $(r_c/3.5)^{10}$, a factor of r_c^{-10} has been excluded from $F_{22}(z)$ in this contour plot. The calculation is based on the "exact" trajectory determined by $V_{iso}(R)$.

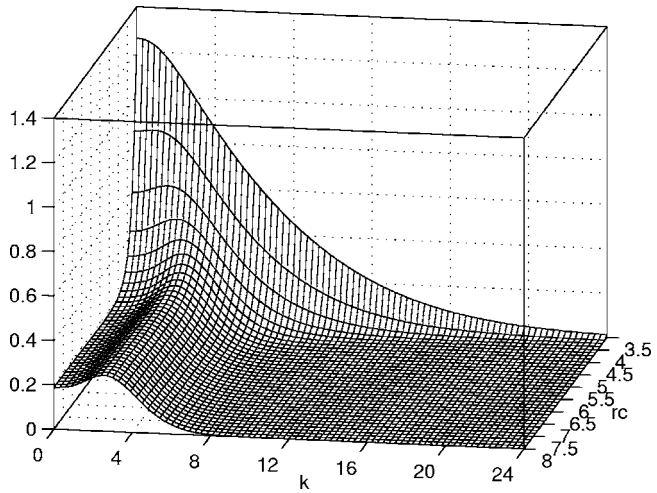

FIG. 7. Fourier transform $H_{22}(k)$ (in ps^{-2}) at 296 K for a molecular pair of N_2-N_2 as a two-dimensional function of z (dimensionless) and r_c (in angstrom). By multiplying $(r_c/3.5)^{10}$, a factor of r_c^{-10} has been excluded from $H_{22}(k)$ in this contour plot. The calculation is based on the "exact" trajectory determined by $V_{iso}(R)$.

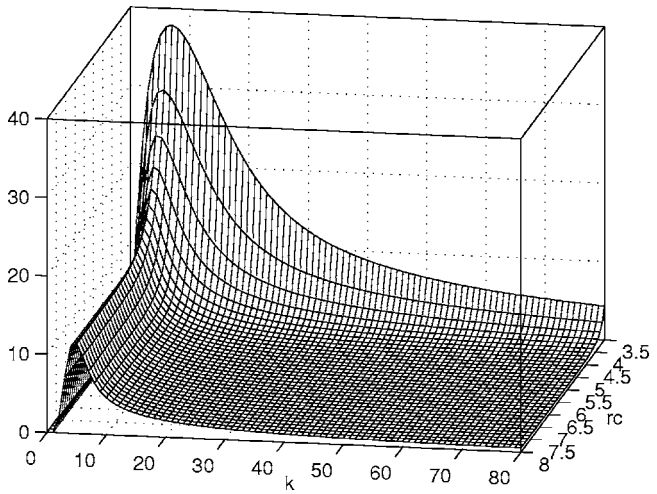

FIG. 8. Cauchy principal integration $I_{22}(k)$ (in ps^{-2}) at 296 K for a molecular pair of N_2-N_2 as a two-dimensional function of z (dimensionless) and r_c (in angstrom). By multiplying $(r_c/3.5)^{10}$, a factor of r_c^{-10} has been excluded from $I_{22}(k)$ in this contour plot. The calculation is based on the "exact" trajectory determined by $V_{iso}(R)$.

later. A very rapid decrease of its magnitude as z increases is clearly shown in the figure. Meanwhile, in order to show how the profile varies with r_c more clearly within a limited scale, $F_{22}(z)$ in this figure and all following are multiplied by a factor of $(r_c/r_0)^{10}$, where r_0 (=3.5 Å) is the starting value of the r_c axis. The factor of r_c^{-10} is a common dependence of those functions on r_c if the leading quadrupole-quadrupole interaction V_{qq} is the only anisotropic potential component. In this latter case, the plotted profiles should not exhibit any r_c dependence. As shown by the figure, the short-range $V_{\text{atom-atom}}$ plays significant role for $F_{22}(z)$ for $z \to 0$ and $r_c \to r_{c,\min}$, and its effects become negligible for $z > 2$ or $r_c > 6.0$ Å. This feature is expected because except at short ranges, V_{qq} dominates. As mentioned above, profiles of $F_{22}(z)$ and other l_1 and l_2 components contain all dynamical information in the time domain necessary in calculating linewidths and shifts.

H. Profiles of $H_{l_1 l_2}(k)$ and $I_{l_1 l_2}(k)$

In this section, we present two contour plots for the Fourier transform functions $H_{l_1 l_2}(k)$ and their corresponding Cauchy principal integrations $I_{l_1 l_2}(k)$. Because $H_{l_1 l_2}(k)$ are even functions of k and $I_{l_1 l_2}(k)$ are odd, we present only half of them along the positive k axis. Again, we select their major components with $l_1=2$ and $l_2=2$ as the example and present $H_{22}(k)$ and $I_{22}(k)$ derived from the "exact" trajectories determined by $V_{iso}(R)$ in Figs. 7 and 8, respectively. As mentioned above, we have excluded a factor of r_c^{-10} from these plots. As shown by Fig. 7, except for $r_c \to r_{c,\min}$, magnitudes of $H_{22}(k)$ increase first as k increases, reach a maximum, and then fall to zero very quickly. This is a clear demonstration that these Fourier transforms are band limited. With respect to the r_c dependence, as long as the values of r_c are beyond 6.0 Å, the profile of $H_{22}(k)$ does not change pattern. Then, as r_c decreases, its magnitude becomes enhanced, especially for small k values. Finally, when $r_c \to r_{c,\min}$, the profile changes completely such that its magnitude increases as much as five to six times. As a result, one can expect that by taking into account the $V_{\text{atom-atom}}$ component in the N_2-N_2 pair, calculated widths will be significantly larger than those derived from the quadrupole-quadrupole interaction V_{qq} alone. In Fig. 8, we show the contour plot for $I_{22}(k)$. As shown in the figure, $I_{22}(k)$ increases from 0 to its maximum as k increases; then, it falls down slowly towards its asymptotic value. Meanwhile, the profile of $I_{22}(k)$ keeps the same pattern for $r_c > 6.0$ Å, increasing as r_c decreases, and enhances dramatically as $r_c \to r_{c,\min}$. Note that for larger r_c values where the influence of $V_{\text{atom-atom}}$ becomes negligible, our calculated profiles of $H_{22}(k)$ and $I_{22}(k)$ match the real and the imaginary parts of the resonance function applicable for V_{qq} exactly.

I. Calculated half-widths from different trajectories

In the present study, to develop a new method to enable one to remove some uncertainties in calculating the widths and shifts, and to use this powerful method to exhibit possible problems existing in current theoretical studies are our main goals. We do not make any attempt to match the experimental data by optimizing potential parameters in the present calculations, rather we simply adopted the potential model used by others. For completeness, however, we do provide experimental data[20] in the following figures. It may appear that the new calculated values are worse than the older ones presented in the literature. But, readers should not use these comparisons as a gauge to judge the accuracy of the present theory because the new results are "true" values representing the current approximations. For example, our calculated results are converged, but we are pretty sure that at least some of the results in the literature are not. If these authors were to take into account more terms to reach the convergence, they should obtain the same values as ours.

We have calculated the Raman Q line widths for N_2-N_2 at 296 K based on the four model trajectories discussed above and we present these results with bold curves in Fig. 9.

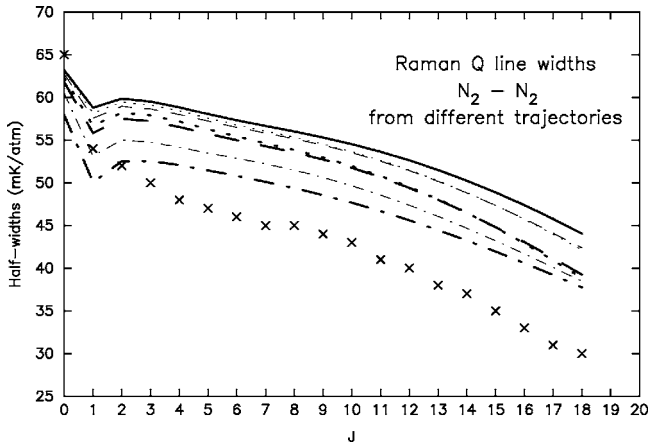

FIG. 9. Calculated Raman Q line half-widths of N_2-N_2 at 296 K from different trajectories. Results derived from the "exact" trajectory determined by $V_{iso}(R)$ are given by a solid. For other trajectories, we plot one bold and one thin line for each of them corresponding to two pair of the LJ parameters: one with $\epsilon=95.2$ K, $\sigma=3.75$ Å and the other with $\epsilon=95.05$ K, $\sigma=3.698$ Å, respectively. Two dotted lines are results based on the "exact" trajectory determined by $V_{LJ}(R)$. Two dot-dashed lines are results from the "parabolic" trajectory with apparent velocity v_c' moving along the straight path. Two dashed ones are from the modified parabolic trajectory. The experimental data are given by $\times$.

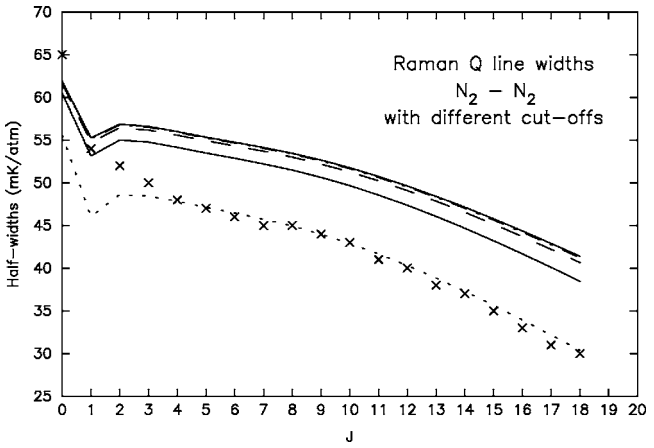

FIG. 10. Calculated Raman Q line half-widths of N_2-N_2 at 296 K with different cutoffs. Results are based on the "parabolic" trajectory with apparent velocity v_c' moving along the straight path. There are two major pairs of l_1 and l_2 taken into account. Theoretical values obtained with the 4th, 6th, 8th, 10th, 12th, and 16th order cutoffs are represented by six curves, from the bottom to the top, respectively. As shown by the figure, the calculated widths become converged only for tenth order or beyond. The fourth-order cutoff used commonly in the literature is too low to reach converged results. The experimental data are given by $\times$.

As shown by the figure, calculated values depend strongly on which trajectory is chosen. The "exact" trajectory determined by $V_{iso}(R)$ produces the largest magnitude, while the first "parabolic" one gives the smallest. Meanwhile, the "exact" trajectory determined by $V_{LJ}(R)$ and the modified parabolic are in between and their differences are very small. It is worth mentioning that the trajectories themselves are not solely responsible for these differences. The poor matching between $V_{iso}(R)$ and the LJ model is another source for differences. In order to show the effect from the LJ parameters, we use better parameters[19] $\epsilon=95.05$ K and $\sigma=3.698$ Å and repeat calculations for those trajectories depending on $V_{LJ}(R)$. For simplicity, we present these results with the same kind of curves, but denote them by thin lines. As shown in Fig. 9, the differences have been reduced significantly. Based on these comparisons, one can draw two conclusions. First of all, calculated results depend significantly on the trajectory. Because the "exact" trajectory determined by $V_{iso}(R)$ is the most realistic it is the best choice in calculating linewidths and shifts. Second, if one chooses another trajectory model, one must be careful to check whether their LJ parameters match $V_{iso}(R)$ well. The LJ parameters should not be treated as free parameters to improve the agreement between theoretical predictions and experimental data. Besides, the total potential should satisfy other criteria such as the second virial coefficient, differential scattering cross section, etc.

In the present study, while we have not carried out the velocity averaging as shown in Eqs. (1) and (2) there is no problem in doing this using the present method. The only thing one needs to do is to select several dozens of values of the velocity and to repeat the calculations of S_1 and S_2 for those specified velocities. Then, by using proper weights from the Maxwell-Boltzmann distribution, one can carry out the averaging over the velocity.

J. Convergence checks

After discussing how to deal with more sophisticated trajectory models and the uncertainties resulting from the selection of the LJ parameters, we would like to use the present method to check the convergence problem which, to the best of our knowledge, has never been thoroughly investigated. As mentioned previously, there are two cutoffs introduced in the calculations, but it is the second cutoff that could cause trouble. Again, we select the Raman Q line width of N_2-N_2 as an example and carry out two checks for the two cutoffs. We use the "parabolic" trajectory with the apparent velocity v_c' moving along a straight path to illustrate our results. In Fig. 10, we present a check for the second cutoff, i.e., by imposing an upper limit for the summation indices w and w' in Eq. (10). Usually, if one chooses 4 as the upper limit of $2w$ and $2w'$, the cutoff is said to be fourth order. This fourth-order cutoff is commonly adopted by many researchers because with the usual methods, it is difficult to use a higher cutoff. In contrast, as explained above, with the present method one can choose any cutoff one wants. Therefore, the present method can serve as a mean to investigate whether calculated results existing in the literature are converged or not. In Fig. 10, we present calculated results derived with six choices: the 4th, 6th, 8th, 10th, 12th, and 16th order cutoffs. From the figure, one can draw two conclusions. The first is that fourth order is too low to reach converged values. The second is that well-converged values can be achieved only from the tenth-order cutoff or higher. This implies that at least for as many cases of practical interest, one is not able to obtain converged results using the usual methods. In summary, there are serious convergence problems exiting in current linewidth and shift theories and results.

With respect to the first cutoff associated with selections of irreducible tensors l_1 and l_2, the situation is much better.

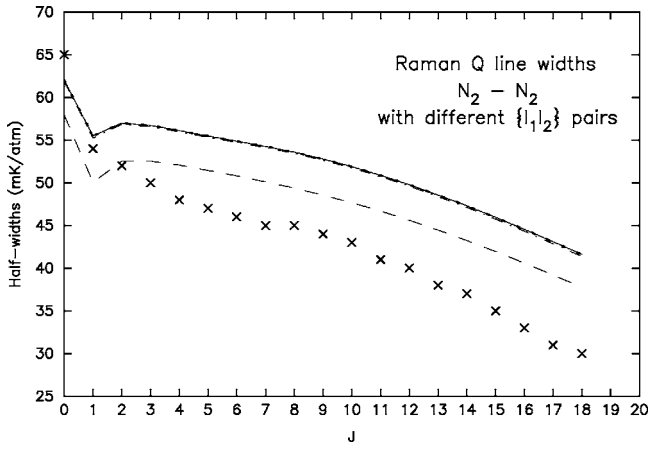

FIG. 11. Calculated Raman Q line half-widths of N_2-N_2 at 296 K with different limitations of the pair of l_1 and l_2 considered in calculations. Results are based on the "parabolic" trajectory with apparent velocity v_c' moving along the straight path. The cutoff used here is the 12th order. There are four choices presented in the figure. The dashed curve is for considering the dominated pair {22} (i.e., $l_1=2$ and $l_2=2$) only. The dot-dashed curve is for two major pairs {22} and {20} which is commonly adopted in literature for N_2-N_2 system. The other two represent results from more pairs to be taken into account in consideration. The dot-dashed one is for six pairs: {22}, {20}, {40}, {24}, {42}, and {06}. The solid line is for nine pairs in which besides those listed six pairs, there are three more pairs {60}, {26}, and {44}. These two curves are indistinguishable. As shown by the figure, one can obtain converged values by including two major pairs. The experimental data are given by ×.

For the N_2-N_2 system, the leading electrostatic interaction is the quadrupole-quadrupole interaction. Therefore, the dominant pair of tensors is $l_1=2$ and $l_2=2$ labeled as {22}. All the other pairs result from the short-range $V_{\text{atom-atom}}$ interaction. Due to the symmetry of the N_2-N_2 system, the next most important pair is {20}. Then, there are four pairs: {40}, {24}, {42}, and {60} at the same level of hierarchy. If one goes further, there are three more pairs: {26}, {62}, and {44}. Accordingly, we carry out calculations with four different selections of $\{l_1 l_2\}$. We first consider only the dominant pair {22}, then the two major pairs {22} and {20}, then six pairs by adding {40}, {24}, {42}, and {60}, and finally all nine pairs listed above. For each of these pairs, we use the 12th order cutoff to do calculations. In Fig. 11, we present our results to show how the values converge as more pairs are taken into account. As shown by the figure, the convergence goes very quickly such that by considering the major two pairs {22} and {20} only, the results are already well converged. It is worth noting that only these two pairs were used in literature for the Raman Q linewidths of the N_2-N_2 system. Therefore, one can conclude that with respect to the first cutoff, there is no convergence problem in previous studies of the Raman Q linewidths for N_2-N_2 or similar systems. Of course, one cannot extrapolate this conclusion to other linewidths or to other systems without performing convergence checks such as discussed here.

Before ending this section, we would like to say a few words about why the convergence problem has remained open for so many years. Of course, it is partially due to the fact that one could not make a complete check because the exact treatment of higher-order cutoffs were not feasible. In the literature, there are some discussions to justify the usage of the fourth-order cutoff. They are based mainly on an estimation of how small the magnitudes of correction terms in the spherical expansion of $V_{\text{atom-atom}}$ would be, in comparison with the leading terms. The key point here is that the smallness of the corrections in itself is not adequate to justify convergence because small neglected terms could still make significant contributions through couplings with stronger terms included.

III. DISCUSSIONS AND CONCLUSIONS

In the present study, based on introducing the coordinate representation and starting calculations of the $\hat{S}$ matrix from the autocorrelation functions, we have developed a new method with which one is able to calculate converged half-widths and shifts no matter how complicated the potential model and trajectory are. This theory enables one to overcome the convergence problem completely. Our calculated results represent "true" values at the adopted level of approximation. Using this method, we have performed convergence checks over the cutoffs and concluded that the commonly employed cutoffs for w and w' are far from adequate as has heretofore been assumed. As a result, one must check carefully whether calculated results are converged or not, compare only converged results with experimental data, and use these latter comparisons to look for directions to make further improvements and refinements of the theory.

Finally, we would like to make some general comments on the approximations currently made in theoretical calculations. It is well known that the calculations of linewidths and shifts are based on several approximations. The binary collision and the impact approximations are two sound ones whose applicability in calculating half-widths and shifts has been well justified. Besides these two, there are others based on the formalism used. Often, these additional approximations are necessary to make practical calculations feasible, but they also inevitably lead to uncertainties in the calculated results. Therefore, in order to provide more reliable theoretical predictions, it is necessary to remove as many of these latter approximations as possible.

Based on previous work,[5] we have removed some approximations that are tacitly incorporated in the RB formalism by an invalid assumption in applying the linked-cluster theorem[21,22] in the derivation. With the present study, we have removed another two approximations: one is related to the cutoffs and the other is associated with the trajectory assumed. However, there are still other approximations remaining. Specifically, we would like to list three major ones which could significantly affect the reliability of calculated results. The first one is the second-order perturbation expansion in the Liouville $\hat{S}$ matrix. So far, for most theoretical calculations, the third-order terms have been ignored. We think that one should begin to consider contributions from these higher-order terms, at least for simple systems. The second one is that we have assumed that the Liouville resolvent operator is diagonal with respect to the line space of the absorber molecule. This assumption is applicable only for well-separated lines. One has to develop a more general formalism such that the line coupling effect can be taken into

account. There have been a number of studies on line coupling,[23,24] but for the most part, these have been concerned primarily with Q branches and far wings of molecular bands. Finally, it has been assumed that the trajectory is determined only by the isotropic part of interaction and the anisotropic part is not considered. We think that this approximation could introduce significant uncertainties in the calculations because the anisotropic interaction does play a significant role in determining the trajectory. As shown by Fig. 9, small changes of the trajectory could cause quite large differences in the corresponding widths and shifts. However, to address this problem presents a big challenge because the coupling between the internal motion and translational motion has to be considered.

It is well known that there are urgent requirements to provide accurate theoretical calculated widths and shifts for diverse applications. But, one has to keep in mind that unless the problems mentioned above and possibly some others have been addressed, there is still much work to be done before one can conclude with certainty that the theoretically calculated values are really reliable.

ACKNOWLEDGMENTS

Two of the authors (Q.M. and R.H.T.) acknowledge financial support from NASA under Grant Nos. NAG5-13337 and FCCS-547. One of the authors (Q.M.) wishes to acknowledge financial support from the Biological and Environmental Research Program (BER), U.S. Department of Energy, Interagency Agreement No. DE-AI02-93ER61744. The authors would like to thank the National Energy Research Supercomputer (Livermore, CA) for computer resources.

[1] P. W. Anderson, Phys. Rev. **76**, 647 (1949).
[2] C. J. Tsao and B. Curnutte, J. Quant. Spectrosc. Radiat. Transf. **2**, 41 (1962).
[3] D. Robert and J. Bonamy, J. Phys. (France) **40**, 923 (1979).
[4] J. Bonamy, D. Robert, and C. Boulet, J. Quant. Spectrosc. Radiat. Transf. **31**, 23 (1984); B. Labani, J. Bonamy, D. Robert, J.-M. Hartmann, and J. Taine, J. Chem. Phys. **84**, 4256 (1986); J.-M. Hartmann, J. Taine, J. Bonamy, B. Labani, and D. Robert, *ibid.* **86**, 144 (1987); B. Labani, J. Bonamy, D. Robert, and J -M. Hartmann, *ibid.* **87**, 2781 (1987).
[5] Q. Ma, R. H. Tipping, and C. Boulet, J. Quant. Spectrosc. Radiat. Transf. (to be published).
[6] *Phenomena Induced by Intermolecular Interactions*, edited by G. Birnbaum (Plenum, New York, 1985).
[7] C. G. Gray and K. E. Gubbins, *Theory of Molecular Fluids* (Clarendon, Oxford, 1984).
[8] R. R. Gamache, R. Lynch, and S. P. Neshyba, J. Quant. Spectrosc. Radiat. Transf. **59**, 319 (1998).
[9] Q. Ma and R. H. Tipping, J. Chem. Phys. **108**, 3386 (1998); Q. Ma and R. H. Tipping, J. Chem. Phys. **111**, 5909 (1999); Q. Ma and R. H. Tipping, J. Chem. Phys. **112**, 574 (2000); Q. Ma and R. H. Tipping, J. Chem. Phys. **116**, 4102 (2002).
[10] Q. Ma and R. H. Tipping, J. Chem. Phys. **117**, 10581 (2002).
[11] H. J. Weaver, *Theory of Discrete and Continuous Fourier Analysis* (Wiley-Interscience, New York, 1989).
[12] P. M. Morse and H. Feshbach, *Methods of Theoretical Physics* (McGraw-Hill, New York, 1953).
[13] S. Green, in *Status and Future Developments in Transport Properties*, edited by W. A. Wakeham, A. S. Dickinson, F. R. W. McCourt, and V. Vesovic (Kluwer Academic Publishers, Netherlands, 1992), p. 257.
[14] J. Buldyreva, S. Benec'h, and M. Chrysos, Phys. Rev. A **63**, 012708 (2000); J. Buldyreva, S. Benec'h, and M. Chrysos, *ibid.* **63**, 032705 (2001).
[15] J. Buldyreva, J. Bonamy, and D. Robert, J. Quant. Spectrosc. Radiat. Transf. **62**, 321 (1999).
[16] A. D. Bykov, N. N. Lavrent'eva, and L. N. Sinitsa, Atmos. Oceanic Opt. **5**, 587 (1992); A. D. Bykov, N. N. Lavrent'eva, and L. N. Sinitsa, *ibid.* **5**, 728 (1992).
[17] H. Goldstein, *Classical Mechanics* (Addison-Wesley, Reading, MA, 1980).
[18] J. P. Looney and G. J. Rosasco, J. Chem. Phys. **95**, 2379 (1991).
[19] J. O. Hirschfelder, C. F. Curtiss, and R. B. Bird, *Molecular Theory of Gases and Liquids* (Wiley, New York, 1964).
[20] L. A. Rahn and R. E. Palmer, J. Opt. Soc. Am. B **3**, 1164 (1986).
[21] C. Bloch, Nucl. Phys. 7, 451 (1958).
[22] R. Kubo, J. Phys. Soc. Jpn. **17**, 1100 (1962).
[23] P. W. Rosenkranz, IEEE Trans. Antennas Propag. **23**, 498 (1975).
[24] A. Levy, N. Lacome, and C. Chackerian, Jr, in *Spectroscopy of the Earth's Atmosphere and Interstellar Medium*, edited by K. N. Rao and A. Weber (Academic, Boston, 1992).